Biosensors and Bioelectronics 26 (2011) 3806–3811

Contents lists available at ScienceDirect

Biosensors and Bioelectronics

journal homepage: www.elsevier.com/locate/bios

Development of an impedimetric aflatoxin M1 biosensor based on a DNA probe and gold nanoparticles

Erhan Dinçkaya[a], Özer Kınık[b], Mustafa Kemal Sezgintürk[c,*], Çağrı Altuğ[a], Aylin Akkoca[a]

[a] Ege University, Faculty of Science, Biochemistry Department, 59100, Bornova-İzmir, Turkey
[b] Ege University, Faculty of Agriculture, Department of Dairy Technology, 59100, Bornova-İzmir, Turkey
[c] Namık Kemal University, Faculty of Arts and Sciences, Chemistry Department, Biochemistry Division, Değirmenaltı, Tekirdağ, Turkey

ARTICLE INFO

Article history:
Received 9 December 2010
Received in revised form 21 February 2011
Accepted 22 February 2011
Available online 1 March 2011

Keywords:
Aflatoxin M1
Electrochemical impedance spectroscopy
Biosensor
Gold nanoparticles
Self-assembled monolayers
Mycotoxins

ABSTRACT

The present work describes the construction and application of a new DNA biosensor for detection of aflatoxin M1. In order to immobilize a thiol-modified single stranded DNA (ss-HSDNA) probe that specifically bound aflatoxin M1, a self-assembled monolayer of cysteamine and gold nanoparticles on the SAM were prepared on gold electrodes, layer-by-layer. The assembly processes of cysteamine, gold nanoparticles, and ss-HSDNA were monitored with the help of electrochemical impedance spectroscopy (EIS) and cyclic voltammetry (CV) techniques. $K_3[Fe(CN)_6]/K_4[Fe(CN)_6]$ solution was used as a redox probe for electrochemical measurements. The biosensor provided a linear response to aflatoxin M1 over the concentration range of 1–14 ng/mL with a standard deviation of ±0.36 ng/mL. Finally, the biosensor was applied to a series of real milk samples.

1. Introduction

Extremely serious human health disorders such as hepatocellular carcinoma, aflatoxicosis, Reye's syndrome and chronic hepatitis are caused by aflatoxins (Deshpande, 2002; Cotty and Garcia, 2007; Gremmels, 2008). The most important form of exposure is consumption of grains contaminated by aflatoxin-producing fungal strains during growth, harvest, or storage. *Aspergillus—Aspergillus flavus*, *Aspergillus parasiticus*, and the rare *Aspergillus nomius* are the main producers of aflatoxins (Bakırcı, 2001; Lopez et al., 2001). When aflatoxins B1 and B2 are ingested by cows, they are converted into their hydroxylated metabolites, which are aflatoxins M1 and M2, respectively (Richard, 2007). Because of the considerable resistance of aflatoxin M1 to industrial processes it may be contained in milk and milk-related products. The chemical structure of aflatoxin M1 is given below.

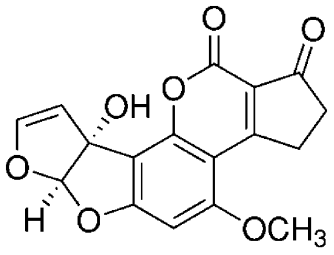

Aflatoxin M1

Van Egmond has reported the acute toxicity of aflatoxin M1. According to this report, aflatoxin M1 can cause vitally important changes in liver parenchymal cells, dissociation of ribosomes from the rough endoplasmic reticulum, and proliferation of the smooth endoplasmic reticulum. Long-term toxicity studies of aflatoxin M1 were reported by van Egmond again. The results concluded that aflatoxin M1 is a potent liver carcinogen (van Egmond, 1983). Moreover, DNA damage and genotoxicity of aflatoxin M1 were evaluated. These studies showed that aflatoxin M1 damaged DNA. Another study showed that it was a genotoxin in mammalian systems in vivo. (Shibahara et al., 1995; Egmond et al., 2007).

Because control of aflatoxin M1 is vitally important, several different measurement techniques have been developed. Most of them require extraction of aflatoxin M1 from its source, purification by removing other substances, and finally quantification.

* Corresponding author. Tel.: +90 282 2933866; fax: +90 282 2643513.
E-mail addresses: msezginturk@nku.edu.tr, msezginturk@hotmail.com (M.K. Sezgintürk).

0956-5663/$ – see front matter © 2011 Elsevier B.V. All rights reserved.
doi:10.1016/j.bios.2011.02.038

Usually, aflatoxin M1 analyses are performed by ELISA (enzyme-linked immunosorbent assay) (Kim et al., 2000; El-Nezami et al., 1995; Thirumala-Devi et al., 2002; Lopez et al., 2003; Rodriguez Velasco et al., 2003; Rastogi et al., 2004; Sarimehmetoglu et al., 2004; Logrieco et al., 2005), TLC (thin layer liquid chromatography) (Sydenham and Dhephard, 1996; Helrich, 1990; Kamkar, 2006) and HPLC (high-performance liquid chromatography) (Cole, 1986; Dragacci et al., 2001; Bognanno et al., 2006). Although the chromatographic methods are well-proven, they have some limitations. For example, they are usually considered as laborious and time-intensive. Moreover, they require expensive equipment and materials. Immunochemical methods based on the high affinity of antigen–antibody interactions provide excellent sensitivity. Different assay techniques utilizing RIA (radioimmunoassay), ELISA, ICA (immunoaffinity column assay), and immunoaffinity flourometric biosensors have been reported (Ricci et al., 2007; Gaag et al., 2003; Chu, 1990; Sibanda et al., 1999; Thirumala-Devi et al., 2002; Magliulo et al., 2005; Radoi et al., 2008; Ricci et al., 2007; Badea et al., 2004; Micheli et al., 2005). In addition, immunoassays integrated with electrochemical, scanning densitometry, colorimetric, chemiluminescent, fluorescence and surface plasmon resonance transducers have also been developed (Ammida et al., 2004; Ho and Wauchope, 2002; Garden and Strachan, 2001; Sapsford et al., 2006; Daly et al., 2000). Parker and Tothill reported an immunosensor based on a competitive reaction between the free aflatoxin M1 in the sample and an aflatoxin M1–horseradish peroxidase conjugate, for an immobilised monoclonal antibody for aflatoxin M1 (Parker and Tothill, 2009). The resulting biosensor was interference free and achieved a limit of detection of 0.039 ng/mL with a linear dynamic detection range up to 1 ng/mL.

In this research, a DNA biosensor was developed to detect aflatoxin M1 in milk and dairy products quickly, practically, and accurately. The novelty of the study is its measurement technique, EIS. In literature, electrochemical impedance spectroscopy was used to analyze aflatoxin M1 for the first time in this study. In this scope, it is hoped that this will lead to the development of biosensors utilizing electrochemical impedance spectroscopy (EIS) to analyze compounds that have restricted catalytic interaction activity such as aflatoxins. In recent years, EIS has become a powerful tool for evaluating many biochemical and biophysical processes. EIS presents analytical solutions for various processes, and in addition, scientific studies such as determining membrane specifications, and biosensor characterization and fabrication can be realized using EIS techniques. Conversely, with enzyme–substrate interactions, biomolecule interactions which have no reaction sequence after binding, such as antigen–antibodies, DNA etc., charge transfer changes occurring after affinity interactions can also be monitored with the help of EIS[3]. A ss-HSDNA, which was specifically bound to aflatoxin M1 was immobilized onto gold electrodes with the help of cysteamine and gold nanoparticles. The differences between before and after binding of aflatoxin M1 to the HSDNA probe were analyzed by cyclic voltammetry and electrochemical impedance spectroscopy techniques. Some important optimization studies were carried out. Then an aflatoxin M1 calibration curve was prepared by considering the differences in electron transfer resistances before and after aflatoxin M1 binding. Real sample analyses were carried out on milk samples.

2. Experimental

2.1. Materials and methods

All chemicals used were of analytical grade and were used as received, without any further purification, and were obtained from Sigma–Aldrich (USA) company. Aflatoxin M1 (produced by *A. flavus*) and 21-mer ss-HSDNA (5′-thiol-$(CH_2)_6$-ACT GCT AGA GAT TTT CCA CAT-3′) were also purchased from Sigma–Aldrich and Thermo Scientific, respectively. All the electrochemical measurements, including electrochemical impedance spectroscopy, were carried out by a Potentiostate/Galvanostate [(AutoLAB, PGSTAT 302 (FRA 2-220, ECD-220 Modules)]. The measurements were controlled with a personal computer running the electrochemical software package of AutoLAB (GPES and FRA) for parameter setup, data acquisition, and processing. A three-electrode configuration was employed in all experiments, with potentials referring to an Ag/AgCl reference electrode. Gold electrodes (Metrohm, Switzerland) and a platinum electrode (Metrohm, Switzerland) were employed as a working and an auxiliary electrode (2.0 ± 0.1 mm in diameter), respectively. All measurements were carried out at a constant temperature with the help of a cryostat (Lauda RE106, Germany). Before every experiment, the gold electrode tips were polished using alumina polishing kits (Metrohm, Switzerland).

2.2. Cleaning procedure for the Au electrode surface

The surfaces of the Au electrodes were first polished with 0.05 μm Al_2O_3 powder and then washed ultrasonically in deionized water for 5 min to remove alumina particles. Then the electrodes were immersed into Piranha (H_2O_2/H_2SO_4, 30/70, v/v) solution for 10 s. Following that, the electrodes were washed with ultra pure water by immersion into water twenty times. In the next step, the surfaces of the electrodes were dried by pure nitrogen stream. This polishing and cleaning procedure was repeated before every electrode preparation step.

2.3. Gold nanoparticle preparation

Gold nanoparticles were prepared according to the literature (Frens, 1973). Briefly, 1 mL of 1% $HAuCl_4$ was added to 90 mL of H_2O at room temperature. After 1 min of stirring, 2.00 mL of 38.8 mM sodium citrate was added. One minute later, 1.00 mL of fresh 0.075% $NaBH_4$ in 38.8 mM sodium citrate was added. The gold nanoparticle solution was stirred for an additional 5 min and stored in a dark bottle at 4 °C.

2.4. Immobilization of 21-mer ss-HSDNA onto Au electrode surface

Firstly, a clean gold electrode was immersed into cystamine solution (10 mM) for 2 h under ambient condition. Then the gold electrode covered by self-assembled monolayer (SAM) of cysteamine was gently washed with absolute ethanol to remove unbounded cysteamine residues. Then the electrode was dried with nitrogen stream. Following that, the modified Au electrode was immersed in the gold nanoparticle solution for 12 h. After this period the electrode was washed with water to remove unbounded gold nano particles. Finally, 10 μl of ss-HSDNA, which was specifically bound with aflatoxin M1 was carefully spread over the Au electrode and allowed to dry at 4 °C for 6 h.

2.5. Electrochemical measurements

Faradaic impedance and cyclic voltammetry measurements were carried out in the presence of 5 mM $K_3[Fe(CN)_6]/K_4[Fe(CN)_6]$ (1:1) solution which served as a redox probe. The redox probe solution was also contained 0.1 M KCl. For all impedance measurements, a DC potential of 0.18 V was used as a bias potential in the frequency range of 100,000 to 0.1 Hz. In the experiments, the alternating voltage was 0.01 V. The impedance data were shown as

Nyquist plots. This is the common representation method of such spectra.

2.6. Measurement procedure

The biosensor based on 21-mer ss-HSDNA was put into the thermostatic reaction cell containing the working buffer (20 mL, 50 mM, pH 7 phosphate buffer). Following that, aflatoxin M1 standard solution was injected into the thermostatic reaction cell and the magnetic stirrer was fixed at a constant speed, and after binding of aflatoxin M1 to the DNA probe, the biosensor was removed from the reaction cell. Then the biosensor was gently immersed into the ultra pure water ten times to remove physically adsorbed aflatoxin M1 molecules. Finally, the biosensor was again put into the cell containing $Fe(CN)_6^{4-/3-}$ redox probe solution and the electrochemical measurements were made as described in the previous section. The differences in charge transfer resistance between the biosensor unbounded and bounded aflatoxin M1 was used to prepare aflatoxin M1 calibration curves.

2.7. Sample preparation procedure

To understand the performance of the biosensor in real sample analysis, a milk sample purchased from a local market was used. In order to remove the milk fat the sample was centrifuged at 6000 rpm for 15 min. After centrifuging, three completely separated phases were obtained. The layer at the top of the centrifuge tube was the layer of fat. At the middle and bottom were cream and milk free from fat, respectively. The milk at the bottom of the tube was used as a sample. Consequently, any possibly negative effect of fat on the electrochemical impedance spectroscopy measurements was avoided.

3. Results and discussion

3.1. Characterization of the biosensor based on 21-mer ss-HSDNA

A self-assembled monolayer of cysteamine was a well-organized layer, which showed a special affinity for gold nanoparticles. Fig. 1A shows cyclic voltammograms (CVs) of the modified gold electrode in 5.0 mM ferricynide/ferrocynide solution.

It is known that the cyclic voltammogram of $Fe(CN)_6^{4-/3-}$ is well defined. We obtained characteristic CV of the $Fe(CN)_6^{4-/3-}$ redox couple at the bare gold electrode. When the electrode was covered by the cysteamine self-assembled monolayer, the peak current was slightly increased because the cysteamine was a positively charged species. Because of that it probably adsorbed the negatively charged ferricyanide to the electrode surface. After formation of cysteamine SAM, gold nanoparticles were attached to the –SH residues. The results revealed that gold nanoparticles had no effect on the peak current of the redox probe. Finally, the DNA probe was immobilized onto the modified gold electrode by the linkage between the gold nanoparticles and the –SH residues of the DNA probe. This resulted in a considerable decrease in the peak current because of the blocking effect of the DNA probe on the diffusion of the $Fe(CN)_6^{4-/3-}$ redox couple.

In electrochemical impedance studies of the biosensor, impedance spectrums were recorded as a complex plane where Z' and Z'' represented the imaginary and real parts of impedance, respectively. The R_{ct} value was obtained by an equivalent circuit model, which was fitted with a commercial software, Autolab data analysis (Eco Chemie, Netherlands). An equivalent circuit was found to fit adequately the data over the entire measurement frequency range. This model is given in Supplemental information Fig. 1. Fig. 1B illustrates the results of impedance on the gold electrode

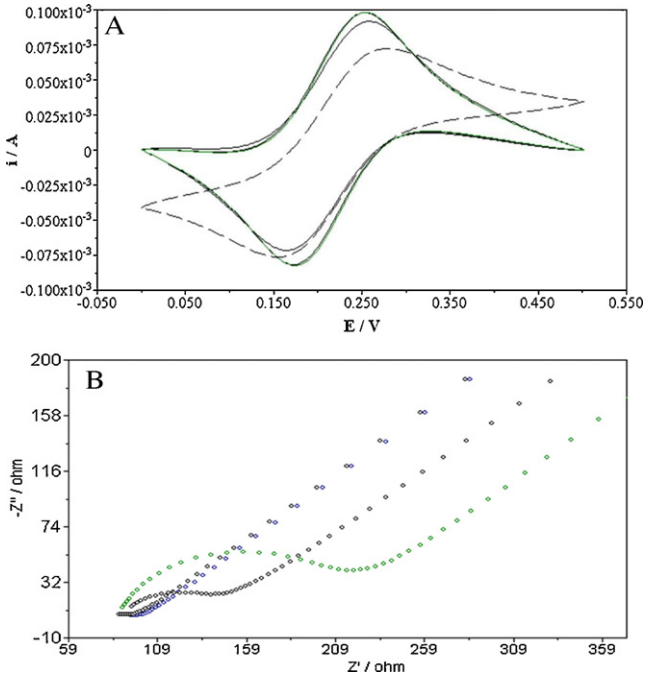

Fig. 1. (A) Cyclic voltammograms for the immobilization steps of the biosensor [dashed line: ss-HSDNA modified electrode, solid line: bare gold electrode, two lines which overlapped: cysteamine and gold nanoparticles modified electrodes. Scanning rate 0.05 V/s]. (B) EIS spectrums for immobilization steps of the biosensor [frequency range: 0.1–100,000 Hz, AC potential: 0.01 V, bias potential: 0.18 V], electrochemical redox probe solution: $Fe(CN)_6^{3-/4-}$, 0.005 M + 0.1 M KCl.

with different layers. The R_{ct} value was first recorded as approximately 83 Ω for the bare gold electrode. The impedance spectrum of the cysteamine-modified gold electrode was an almost straight line. It was influenced by an effect stabilizing the electrostatic interaction between the electrode surface and the redox probe. Moreover, it caused a small increase in the thickness of the surface. The gold nanoparticles did not alter the R_{ct} value. Due to the non-conductivity of HS-DNA probe, after application of the DNA probe, the electron-transfer of $[Fe(CN)_6]^{4-/3-}$ was blocked and R_{ct} increased remarkably. EIS data were consistent with the results obtained from cyclic voltammetry experiments.

The electroactive surface area of the biosensor was calculated according to the Randles–Sevcik equation;

$$I_p = 2.69 \times 10^5 A n^{3/2} D_0^{1/2} \nu^{1/2} C_0$$

where I_p, A, n, D_0, ν and C_0 represent the redox peak current (A), the effective surface area of the electrode (cm^2), electrons per molecule oxidized or reduced ($n = 1$), the diffusion coefficient of $K_3Fe(CN)_6$ in 0.1 M KCl (0.673×10^{-5} cm^2 s^{-1}) (Chailapakul et al., 2000), the scan rate (V s^{-1}) and the concentration of redox species (mol cm^{-3}). According to this equation, the electroactive surface area of the biosensor was 0.043 cm^2.

3.2. Optimization of the biosensor based on 21-mer ss-HSDNA

3.2.1. Optimization studies of the biosensor

The working conditions for the biosensor were examined in terms of temperature, stirring rate, and DC-potential in Faradaic impedance measurements. A discussion of this appears below.

The effect of temperature on the biosensor response was investigated using the temperatures of 20–35 °C. Aflatoxin M1 calibration graphs drawn using different temperatures are given in Fig. 2.

The results revealed that the temperature considerably affected the biosensor performance. Typically, when the temperature was

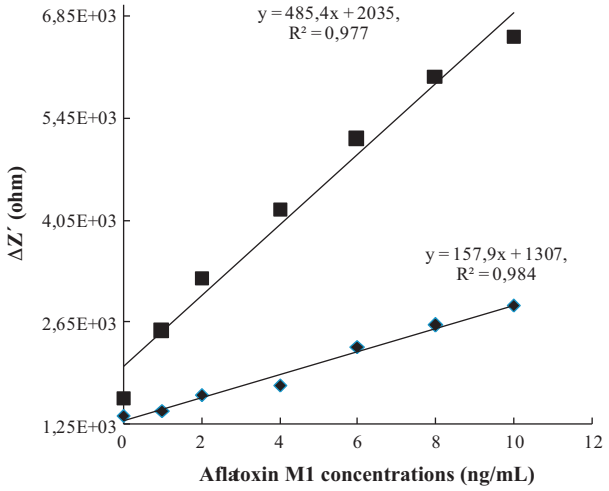

Fig. 2. The effect of temperature on the biosensor [temperatures: (■) 35 °C, (♦) 20 °C. Electrochemical redox probe solution: $Fe(CN)_6^{3-/4-}$, 0.005 M + 0.1 M KCl, frequency range: 0.1–100,000 Hz, AC potential: 0.01 V, bias potential: 0.18 V, 35 °C].

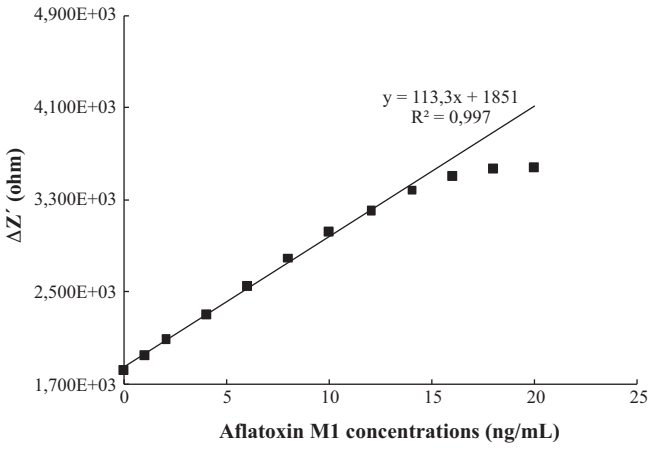

Fig. 4. Calibration curve for aflatoxin M1 [working conditions: stirring rate: 100 rpm, electrochemical redox probe solution: $Fe(CN)_6^{3-/4-}$, 0.005 M + 0.1 M KCl, frequency range: 0.1–100,000 Hz, AC potential: 0.01 V, bias potential 0.18 V, 35 °C].

below 35 °C R_{ct} values decreased by at least 65% for high aflatoxin M1 concentrations. For relatively low concentrations the decrease rate was about 40%. It is likely that the temperature increased the movement of the molecules and of course the kinetic energy to transport them onto the electrode surfaces effectively. Consequently, working temperature was chosen as 35 °C.

The effect of magnetic stirring at intervals from 100 to 300 rpm on the biosensor response time was investigated. The calibration curves obtained in these stirring conditions are shown in Fig. 3.

The experiments showed that the stirring procedure was very important. It was observed that an increase in the rate of stirring resulted in an increase in charge transfer resistance. Moreover, increasing the stirring rate to over 300 rpm caused the results to be converted into a meaningless shape. It is likely that at over 300 rpm, the bioactive layer of the biosensor was physically destroyed because of the high stirring rate. The impedance variations between the two standard concentrations were very low when we worked at the speed of 100 rpm. This made obtaining sensitive and accurate results difficult with the biosensor. Finally, the best results were obtained by stirring the incubation buffer at a rate of 300 rpm.

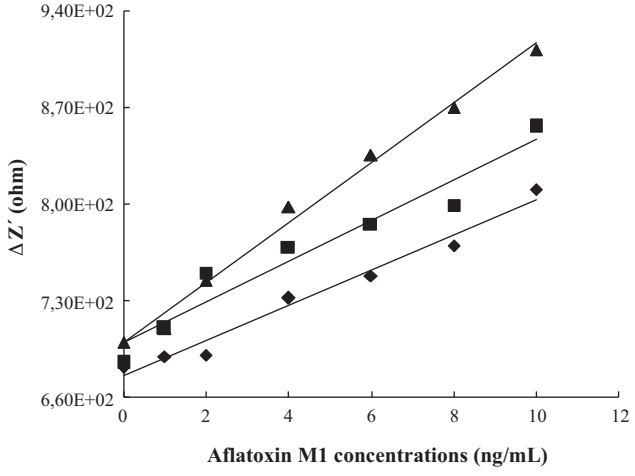

Fig. 3. The effect of stirring rate on the biosensor response and bioactive layer [stirring rates (rpm): (▲) 300, (■) 200, (♦) 100. Electrochemical redox probe solution: $Fe(CN)_6^{3-/4-}$, 0.005 M + 0.1 M KCl, frequency range: 0.1–100,000 Hz, AC potential: 0.01 V, bias potential: 0.18 V].

The other important parameter optimized was the DC potential applied to the system. This DC potential value is also referred to as the bias potential. From the Lissajous analyses for electrochemical impedance spectroscopy, it is clear that the input signal can be represented by;

$$V = v + \Delta V \cos(2\pi f\, t) \quad (1)$$

where v is an applied bias potential and ΔV is the amplitude of the sinusoidal perturbation (Orazem and Tribollet, 2008). We know that the current response is dependent on the characteristics of the system under study. Moreover, the current density associated with the capacitive charging of the electrode can be expressed as;

$$i_c = -C_{dl} dV/dt = 2\pi f\ \Delta V\ C_{dl} \sin(2\pi f\, t) \quad (2)$$

where it accounts for the difference in the direction of the potential difference between that used for the Faradaic and that used for the charging currents. By solution of Eqs. (1) and (2), the value of charge transfer resistance can be given by;

$$R_{ct} = \frac{1}{[(b_a n F K_a \exp(b_a v)) + (b_c n F K_c \exp(-b_c v))]} \quad (3)$$

As can be understood from Eq. (3), charge transfer resistance is dependent on the DC potential applied to the system. Our results showed that Nyquist ($Z' - Z''$) diagrams obtained with different bias potentials indicated that an increase in the potential resulted in a considerable decrease in the R_{ct} value of the biosensor. This result was in good agreement with Eq. (3) because according to Eq. (3), an increase in the DC potential applied to the system should cause a decrease in the charge transfer resistance. Moreover, aflatoxin M1 calibration graphs drawn by using a high DC potential had a better linearity than when using lower DC potentials than 0.1 V. We used a voltage of 0.18 V as the DC potential applied to the system.

3.3. Analytical characteristics of the biosensor

Under the optimal conditions, aflatoxin M1 was detected and quantified by the biosensor developed. As shown in Fig. 4, the part of real impedance increased when the increased aflatoxin M1 was added to the reaction cell.

The response curve showed a linear range from 1 to 14 ng/mL. The regression equation was $y = 113.32x + 1851.2$ with a correlation coefficient of 0.9972, where y was the difference in Z' between

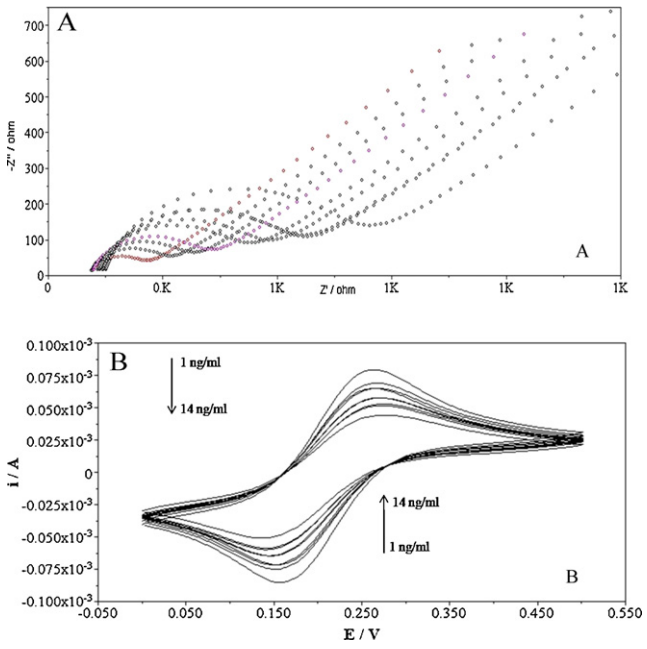

Fig. 5. Cyclic voltammograms (A) and EIS spectrums (B) for aflatoxin M1 concentrations [scanning rate for CV: 0.05 V/s.] [frequency range: 0.1–100,000 Hz, AC potential: 0.01 V, bias potential: 0.18 V] Electrochemical redox probe solution: $Fe(CN)_6^{3-/4-}$, 0.005 M + 0.1 M KCl, 35 °C.

before and after aflatoxin M1 injection, and *x* was aflatoxin M1 concentration. Each measurement was performed at least for three times. For preparation of the curve, average values belonging to each concentration were used. Besides standard deviations for aflatoxin M1 concentrations of 1, 2, 4, 6, 8, 10, 12, 14 ng/mL were 2.45%, 3.1%, 2.68%, 4.6%, 4.4%, 4%, 3.86%, and 4.1%, respectively. Fig. 5A shows the Nyquist plot diagrams of the biosensor for different aflatoxin M1 concentrations. It was observed that the semi-circle diameter in the Nyquist plot increased with increasing aflatoxin M1 concentration. The low frequency ranges were particularly suitable for concentration-dependent impedance measurements.

Moreover, the cyclic voltammograms obtained for different aflatoxin M1 concentrations were in good agreement with impedance measurements. The results are given in Fig. 5B. Peak currents were noticeably decreased with an increase in aflatoxin M1 concentration. The blocking effect of aflatoxin M1 on charge transfer to the electrode surface became clear through cyclic voltammetry measurements.

Assay variances were evaluated by the repeatability study. A standard sample was analyzed five times for aflatoxin M1 standard with a concentration of 6 ng/mL. The average value, standard deviation, and variation coefficient were 5.8 ng/mL, ±0.36 ng/mL, and 6.2%, respectively. The results indicated that the anti-aflatoxin M1 antibody-based biosensor was very reliable with regard to repeatability.

The reproducibility of the biosensor preparation process was evaluated by preparing the calibration graphs and linear detection ranges for aflatoxin M1 consecutively under the same experimental conditions. The results are summarized in Table 1 below.

The results showed that the biosensor reported here can be utilized for aflatoxin M1 detection and quantification.

A determined unit of aflatoxin M1-spiked milk sample was analyzed with the help of the biosensor. The results are shown in Table 1.The experimental results indicated a good recovery. These results showed that the proposed biosensor can be applied successfully for the determination of aflatoxin M1, impedimetrically.

Table 1
The reproducibility of the biosensor based on ss-HSDNA.

Biosensors	R^2	Linear ranges (ng/mL)
1	0.9913	1–14
2	0.9993	1–14
3	0.9922	1–14
4	0.9890	1–14
5	0.9244	1–14

Aflatoxin M1 detection in milk sample spiked with aflatoxin M1 by the biosensor

Aflatoxin M1 (ng/mL)[a]				
Added	Found by the biosensor	% Recovery after extraction	% Relative difference	Standard deviation
0.4	0.428	107	7	4.25

[a] The average of six measurements; these studies were done using six different electrodes.

4. Conclusion

In summary, we have developed an immobilization procedure to construct a DNA biosensor by self-assembled monolayers of cysteamine and gold nanoparticles. Cysteamine and gold nanoparticles should improve the charge transfer of the redox probe through the electrode surface. Electrochemical impedance spectroscopy and cyclic voltammetry were successively employed to elucidate the charge transfer changes occurring during the preparation and utilization of the biosensor-based DNA probe. Electrochemical impedance spectroscopy, in fact, was a relatively time-consuming method. For example, to take an impedance spectrum within a current region of frequencies required 10–15 min. However, this method is a very effective tool for probing the characteristics of a surface modified electrode. Moreover, it is certainly possible to make quantitative analyses by electrochemical impedance spectroscopy. The biosensor reported here is a good example of an interaction between aflatoxins and DNA on the gold electrode surface. Moreover, the biosensor exhibited good analytical characteristics, such as higher affinity of aflatoxin M1 towards the DNA probe, a low quantification limit, and good repeatability and reproducibility. Finally, the biosensor was used for analysis of a series of real samples.

Acknowledgements

This study was supported by TÜBİTAK (The Scientific and Technological Research Council of Turkey, Project number: 106T 367) and EBİLTEM (Ege University of Research and Application Center of Science and Technology, Project number: 2007 BİL 013).

Appendix A. Supplementary data

Supplementary data associated with this article can be found, in the online version, at doi:10.1016/j.bios.2011.02.038.

References

Ammida, N.H.S., Micheli, L., Palleschi, G., 2004. Anal. Chim. Acta 520, 159–164.
Badea, M., Micheli, L., Messia, M.C., Candigliota, T., Marconi, E., Mottram, T., Velasco-Garcia, M., Moscone, D., Palleschi, G., 2004. Anal. Chim. Acta 520, 141–148.
Bakırcı, I., 2001. Food Control 12, 47–51.
Bognanno, M., La Fauci, L., Ritieni, A., Tafuri, A., De Lorenzo, A., Micari, P., Di Renzo, L., Ciappellano, S., Sarullo, V., Galvano, F., 2006. Mol. Nutr. Food Res. 50, 300–305.
Chailapakul, O., Popa, E., Tai, H., Sarada, B.V., Tryk, D.A., Fujishima, A., 2000. Electrochem. Commun. 2 (6), 422–426.
Chu, F.S., 1990. Vet. Hum. Toxicol. 32, 42–50.
Cole, R.J., 1986. Modern Methods in the Analysis and Structural Elucidation of Mycotoxins. Academic Press Inc., Orlando.
Cotty, P.J., Garcia, R.J., 2007. Int. J. Food Microbiol. 119, 109–115.

Daly, S.J., Keating, G.J., Dillon, P.P., Manning, B.M., O'Kennedy, R., Lee, H.A., Morgan, M.R.A., 2000. J. Agric. Food Chem. 48, 5097–5104.
Deshpande, S.S., 2002. Handbook of Food Toxicology. In: Deshpande, S.S. (Ed.), Fungal Toxins. Marcel Decker, New York, pp. 387–456.
Dragacci, S., Grosso, F., Gilbert, J., 2001. J. Assoc. Off. Anal. Chem. Int. 84, 437–443.
Egmond, H.P., Schothorst, R.C., Jonker, M.A., 2007. Anal. Bioanal. Chem. 389, 147–157.
El-Nezami, H.S., Nicoletti, G., Neal, G.E., Donohue, D.C., Ahokas, J.T., 1995. Food Chem. Toxicol. 33, 173–179.
Frens, G., 1973. Nat. Phys. Sci. 241, 20–22.
Gaag, B., Spath, S., Dietrich, H., Stigter, E., Boonzaaijer, G., Osenbruggen, T., Koopal, K., 2003. Food Control 14, 251–254.
Garden, S.R., Strachan, N.J.C., 2001. Anal. Chim. Acta 444, 187–191.
Gremmels, J.F., 2008. Food Addit. Contam. 25, 172–180.
Helrich, K., 1990. Official Methods of Analysis—Food composition; Additives; Natural contaminants, vol. 2. Association of Official Analytical Chemists Inc., USA.
Ho, J.A.A., Wauchope, R.D., 2002. Anal. Chem. 74, 1493–1496.
Kamkar, A., 2006. Food Control 17, 768–775.
Kim, E.K., Shon, D.H., Ryu, D., Park, J.W., Hwang, H.J., Kim, Y.B., 2000. Food Addit. Contam. 17, 59–64.
Logrieco, A., Arrigan, D.W.M., Brengel-Pesce, K., Siciliano, P., Tothill, I.E., 2005. Food Addit. Contam. 22, 335–344.
Lopez, C., Ramos, L., Ramadan, S., Bulacio, L., Perez, J., 2001. Int. J. Food Microbiol. 64, 211–215.
Lopez, C.E., Ramos, L.L., Ramadán, S.S., Bulacio, L.C., 2003. Food Control 14, 31–34.
Magliulo, M., Mirasoli, M., Simoni, P., Lelli, R., Portanti, O., Roda, A., 2005. J. Agric. Food Chem. 53, 3300–3305.
Micheli, L., Grecco, R., Badea, M., Moscone, D., Palleschi, G., 2005. Biosens. Bioelectron. 21, 588–596.
Parker, C.O., Tothill, I.E., 2009. Biosens. Bioelectron. 24, 2452–2457.
Radoi, A., Targa, M., Prieto-Simon, B., Marty, J.L., 2008. Talanta 77, 138–143.
Rastogi, S., Dwivedi, P.D., Khanna, S.K., Das, M., 2004. Food Control 15, 287–290.
Ricci, F., Volpe, G., Micheli, L., Palleschi, G., 2007. Anal. Chim. Acta 605, 111–129.
Richard, J.L., 2007. Int. J. Food Microbiol. 119, 3–10.
Rodriguez Velasco, M.L., Calonge Delso, M.M., Ordonez Escudero, D., 2003. Food Addit. Contam. 20, 276–280.
Sapsford, K.E., Taitt, C.R., Fertig, S., Moore, M.H., Lassman, M.E., Maragos, C.A., Shriver-Lake, L.C., 2006. Biosens. Bioelectron. 21, 2298–2305.
Sarimehmetoglu, B., Kuplulu, O., Celik, T.H., 2004. Food Control 15, 45–49.
Shibahara, T., Ogawa, H.I., Ryo, H., Fujikawa, K., 1995. Mutagenesis 10 (3), 161–164.
Sibanda, L., De Saeger, S., Van Peteghem, C., 1999. Int. J. Food Microbiol. 48, 203–209.
Sydenham, E.W., Dhephard, G.S., 1996. Progress in Food Contamination Analysis. Blackie Academic and Professional, London.
Thirumala-Devi, K., Mayo, M.A., Hall, A.J., Craufurd, P.Q., Wheeler, T.R., Waliyar, F., Subrahmanyam, A., Reddy, D.V.P., 2002. J. Agric. Food Chem. 50, 933–937.
Orazem, M.E., Tribollet, B., 2008. Electrochemical Impedance Spectroscopy. John Wiley & Sons, Hoboken, New Jersey.
van Egmond, H.P., 1983. Food Chem. 11, 289–307.